Science of the Total Environment 806 (2022) 150580

Contents lists available at ScienceDirect

Science of the Total Environment

journal homepage: www.elsevier.com/locate/scitotenv

Climate change impacts on wind energy resources in North America based on the CMIP6 projections

A. Martinez [a], G. Iglesias [a,b,*]

[a] School of Engineering and Architecture & MaREI, Environmental Research Institute, University College Cork, College Road, Cork, Ireland
[b] University of Plymouth, School of Engineering, Computing & Mathematics, Marine Building, Drake Circus, Plymouth PL4 8AA, United Kingdom

HIGHLIGHTS

- Climate change impacts on future wind energy in North America are investigated.
- Two of the novel Shared Socioeconomic Pathways scenarios were considered.
- Method based on multi-model ensemble, with 5 models selected from 18 on performance
- Overall power density drop of ~15% by 2100 in worst case, reaching 40% in some regions
- Increased intra-annual variability, with monthly averages changing by up to +120%, −60%

GRAPHICAL ABSTRACT

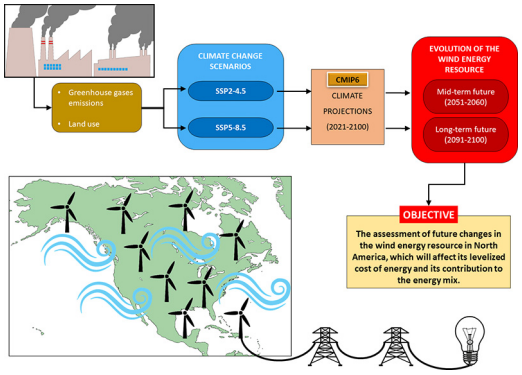

ARTICLE INFO

Article history:
Received 1 June 2021
Received in revised form 1 September 2021
Accepted 21 September 2021
Available online 27 September 2021

Editor: Ouyang Wei

Keywords:
Wind energy
Offshore wind
Wind power
Marine renewable energy
Shared socioeconomic pathways
Multi-model ensemble

ABSTRACT

The mid- and long-term evolution of wind energy resources in North America is investigated by means of a multi-model ensemble selected from 18 global climate models. The most recent scenarios of greenhouse gases emissions and land use, the Shared Socioeconomic Pathways (SSPs), are considered – more specifically, the SSP5-8.5 (intensive emissions) and SSP2-4.5 (moderate emissions). In both scenarios, onshore wind power density in the US and Canada is predicted to drop. Under SSP5-8.5, the reduction is of the order of 15% overall, reaching as much as 40% in certain northern regions – Quebec and Nunavut in Canada and Alaska in the US. Conversely, significant increases in wind power density are predicted in Hudson Bay (up to 25%), Texas and northern Mexico (up to 15%), southern Mexico and Central America (up to 30%). As for the intra-annual variability, it is poised to rise drastically, with monthly average wind power densities increasing up to 120% in certain months and decreasing up to 60% in others. These changes in both the mean value and the intra-annual variability of wind power density are of consequence for the Levelised Cost of Energy from wind, the planning of future investments and, more generally, the contribution of wind to the energy mix.

1. Introduction

According to the Global Wind Report 2021 (Global Wind Energy Council, 2021), North America has replaced Europe as the second-largest regional market for new wind power installations in 2020, led by the US with a record 17 GW of newly installed capacity. Canada

* Corresponding author.
E-mail address: gregorio.iglesias@ucc.ie (G. Iglesias).

https://doi.org/10.1016/j.scitotenv.2021.150580

(CanWEA, 2021) currently ranks 9th in the world in total wind power capacity. Mexico, ranked 4th in America (Hernández-Escobedo et al., 2018), is also allocating significant investments to wind power (Mordor Intelligence, 2021). These developments in North America occur in the context of very rapid development globally. Indeed, 2020 was a record year, with no less than 93 GW of newly installed capacity worldwide. However, it is clear from the Global Wind Report that this development must be further expanded to meet the world's climate targets of zero emissions (Global Wind Energy Council, 2021).

Recently, the scope of the energy sector has broadened thanks to the emergence of offshore energies, e.g., wind (Stelzenmüller et al., 2021; Pınarbaşı et al., 2019; Château et al., 2012), wave (Veigas et al., 2015; Bergillos et al., 2019; Rodriguez-Delgado et al., 2018), tidal (Ramos et al., 2014; Greaves and Iglesias, 2018). Offshore wind energy, in particular, is receiving a great deal of attention and developing rapidly, especially in Europe and China. Recently, the US has approved the first large-scale offshore wind farm off the coast of Massachusetts, with 84 turbines and an installed capacity of approximately 800 MW. With wind turbines mounted on bottom-fixed structures, e.g., jackets (Perez-Collazo et al., 2018) or monopiles (Perez-Collazo et al., 2019; Negro et al., 2017), and floating structures, e.g., spar-buoys (Tomasicchio et al., 2018), tension-leg (Sclavounos et al., 2010) and semi-submersible platforms (Jonkman and Matha, 2010), the greater, less variable offshore wind resource is more and more attractive. Furthermore, offshore renewable energy is emerging as a great alternative for remote locations, e.g., small islands (Veigas and Iglesias, 2015), and presents great opportunities for combined exploitation, e.g., wind-wave (Astariz and Iglesias, 2016) and wind-solar (López et al., 2020). All things considered, the current trends and the new technological solutions anticipate a substantial development in the upcoming years (Rand and Hoen, 2017).

The wind resource itself is a fundamental aspect in the viability of future projects (Ulazia et al., 2017) owing to its influence on the levelised cost of energy (Castro-Santos et al., 2016). Atmospheric patterns are expected to shift as a consequence of climate change (Rockel and Woth, 2007). Given the cubic relationship between wind speed and wind power density, even not-so-large changes in the wind climate have the potential to produce significant impacts on wind resources. Consequently, areas with a well-developed wind power industry may see their resources decrease; conversely, areas which have received scant attention so far may become of interest for future projects. It follows that assessing the evolution of the wind energy resource under climate change is fundamental to the planning of future wind energy projects.

The earliest works addressing the impacts of climate change on wind speeds were based on the climate change scenarios A2 and B2 of cumulative greenhouse gases (GHG) emissions (Räisänen et al., 2004), proposed by the Intergovernmental Panel on Climate Change (IPCC) (IPCC, 2001). The evolution of surface wind speed was subsequently studied considering the SRES-A1B climate change scenario of the Coupled Model Intercomparison Project Phase 3 (CMIP3) at a global scale (McInnes et al., 2011) and, specifically, in the continental US by downscaling a global climate model (GCM) with the WRF model (Liu et al., 2014). Considering regional climate models (RCMs) from the North America Regional Climate Change Assessment Program (NARCCAP) and future climate projections with a high GHG emissions scenario (SRES-A2), the wind power potential was studied in the US (Pryor and Barthelmie, 2011; Johnson and Erhardt, 2016). More recently, the impacts of climate change on surface wind speed over North America (Kulkarni and Huang, 2014) were assessed considering five different GCMs involved in the 5th phase of the Coupled Model Intergovernmental Panel on Climate Change (CMIP5), which uses the representative concentration pathways (RCPs) climate change scenarios (Moss et al., 2010). Even though the climate change scenario with intensive GHG was considered (Kulkarni and Huang, 2014), negligible to moderate changes in surface wind speed were found in Central and East-Central US. Finally, offshore wind speeds were investigated using 12 RCMs of the Coordinated Regional Climate Downscaling Experiment (CORDEX) (Costoya et al., 2020).

Recently, the 6th phase of the Coupled Model Intercomparison Project (CMIP6) released an extensive number of GCMs (Eyring et al., 2016). Within this project, a prominent position is occupied by the Scenario Model Intercomparison Project (ScenarioMIP), which provides climate projections based on the most updated scenarios of future GHG emissions and land use, the Shared Socioeconomic Pathways (SSPs) (Riahi et al., 2017). These GCMs were successfully employed to study changes in wind speed and wind power density in China (Wu et al., 2020), offshore China (Zhang and Li, 2021), the Northwestern Passage (Qian and Zhang, 2021) and Europe (Martinez and Iglesias, 2021). In the latter study, a reduction of approximately 15% in mean wind power density was predicted for Central Europe, with strong decreases of up to 35% in the Mediterranean Basin, and an overall increase in the intra-annual variability (Martinez and Iglesias, 2021). It was shown that the SSPs climate change scenarios anticipate greater changes in wind energy than the previous climate change scenarios, the RCPs.

The evolution of the wind energy resource in North America under these novel climate change scenarios has not been studied so far – and therein lies the motivation of this work. For this purpose, 18 GCMs participating in the ScenarioMIP activity of the CMIP6 are considered. Changes in mean wind power density and temporal variability of the wind resource are assessed in the mid-term and long-term future. GCMs providing projections of daily wind data are considered, and a multi-model ensemble is constructed with those that are found to best reproduce past-present conditions. Furthermore, the use of daily data enables a more accurate analysis of the evolution of the intra-annual variability of wind power, including seasonal and monthly timescales.

The paper is structured as follows. In Section 2, the data and methods used in this work are presented. In Section 3, the evolution of the mean wind power density and its temporal and intra-annual variability is analysed in detail. Finally, in Section 4, conclusions are drawn.

2. Materials and methods

2.1. Region of study and global climate models

The region considered in this study is defined by latitude and longitude in the ranges (12°N, 72°N) and (45°W, 165°W), respectively. Data of wind climate projections from the GCMs framed in the CMIP6 activities are used. Near-surface (10 m height) data of daily averaged wind speed are used and compared against historical data to assess changes in wind energy. The use of near-surface wind speed as a reference is a common practice in this type of study. Wind speeds at different heights are highly correlated and can be obtained following the Hellman exponent and wind gradient equation (Carvalho et al., 2017).

In this study, two different scenarios of climate change are considered: SSP2-4.5 and SSP5-8.5 (O'Neill et al., 2016). SSP2-4.5 represents an intermediate scenario, in which current tendencies in climate change remain constant, leading to a forcing pathway of 4.5 Wm^{-2} in 2100. SSP5-8.5 represents a scenario in which no policies regarding the emission of GHGs are applied, leading to an intensive fossil-fuel consumption resulting in a forcing pathway of 8.5 Wm^{-2} in 2100 (Riahi et al., 2017).

The 18 GCMs involved in the CMIP6 activities providing data on future projections of daily-averaged, near-surface wind data in both climate change scenarios (SSP2-4.5 and SSP5-8.5) are listed in Table 1.

2.2. Data validation

In order to study the performance of the GCMs listed in Table 1, historical data (2005-2014) of the different GCMs are compared against reanalysis data from the ERA-5 database from the European Centre for Medium-Range Weather Forecasts (ECMWF) (Hersbach and Dee, 2016). The ERA products have been the official validation databases

Table 1
GCMs framed in the CMIP6 considered in the study.

Centre	Model	Resolution (lat × lon)	Reference
Alfred Wegener Institute (Germany)	AWI-CM-1-1-MR	0.9375° × 0.9375°	(Semmler et al., 2019)
Beijing Climate Center (China)	BCC-CSM2-MR	1.12° × 1.125°	(Xin et al., 2019)
Canadian Centre for Climate Modelling and Analysis (Canada)	CanESM5	1.775° × 2.1825°	(Swart et al., 2019)
Chinese Academy of Sciences (China)	FGOALS-f3-L	1° × 1.25°	(Yu, 2019)
Commonwealth Scientific and Industrial Research Organization (Australia)	ACCESS-CM2	1.25° × 1.875°	(Dix et al., 2019)
EC-EARTH-CONSORTIUM (Europe)	EC-Earth3	0.7° × 0.7031°	(EC-Earth Consortium, 2019)
Institute for Numerical Mathematics (Russia)	INM-CM4-8	1.5° × 2°	(Volodin et al., 2019a; Volodin et al., 2019b)
Institute for Numerical Mathematics (Russia)	INM-CM5-0	1.5° × 2°	(Volodin et al., 2019c; Volodin et al., 2019d)
Institut Pierre Simon Laplace (France)	IPSL-CM6A-LR	1.2676° × 2.5°	(Boucher et al., 2019)
JAMSTEC (Japan Agency for Marine-Earth Science and Technology) (Japan)	MIROC6	1.4° × 1.4063°	(Shiogama et al., 2019)
Max Planck Institute for Meteorology (Germany)	MPI-ESM1-2-HR	0.93° × 0.9375°	(Schupfner et al., 2019)
Max Planck Institute for Meteorology (Germany)	MPI-ESM1-2-LR	1.85° × 1.875°	(Wieners et al., 2019a; Wieners et al., 2019b)
Meteorological Research Institute (Japan)	MRI-ESM2-0	1.12° × 1.125°	(Yukimoto et al., 2019)
National Center for Atmospheric Research (USA)	CESM2-WACCM	0.9424° × 1.25°	(Danabasoglu, 2019)
NorESM Climate modelling Consortium (Norway)	NorESM2-MM	0.9424° × 1.25°	(Bentsen et al., 2019)
National Institute of Meteorological Sciences/Korea Meteorological Administration (Republic of Korea)	KACE-1-0-G	1.25° × 1.875°	(Byun et al., 2019)
NOAA-GFDL (USA)	GFDL-CM4	1° × 1.25°	(Guo et al., 2018)
NOAA-GFDL (USA)	GFDL-ESM4	1° × 1.25°	(John et al., 2018)

for the CMIP downscaling initiatives (Gutowski et al., 2016) and have been widely used as a reference in previous works (Carvalho et al., 2017; Brands et al., 2013; Dosio et al., 2015; Bloom et al., 2008). The ERA-5 being the most up-to-date ERA product and the most widely recognised database in reanalysis products, its choice is justified.

In this study, data of wind speed projections are compared against historical data of the same GCM. It is therefore of interest to assess distributional differences rather than differences in mean values (bias). For this reason, the Kolmogorov-Smirnov (K—S) test is employed in the region studied. The K—S test examines the null hypothesis of two different sample data belonging to the same distribution against the alternative that they do not (Wilks, 2011).

First, since all different models present different resolutions, the 18 GCMs listed in Table 1 are remapped into a regular 1.5° × 1.5° grid following a first-order conservative remapping, maintaining the flux integrals (Jones, 1999). Second, since daily data on atmospheric variables are greatly seasonal-dependent, the K—S test is applied to the time series after subtracting the seasonal mean (bias) in each time step, thus obtaining centred time series with zero mean. By eliminating the bias, the K—S test has been proved to detect distributional differences in higher-order moments, and it is a common practice in downscaling approaches (Brands et al., 2013). The K—S test is thus applied to the unbiased historical data from the 18 GCMs listed in Table 1 against the unbiased ERA-5 reanalysis data covering the same time period at a significant level of 5%. The performance of the GCMs is measured according to the number of points in the region studied that are statistically similar to the their ERA-5 counterparts – displayed in Table 2 as a percentage of the total number of points.

2.3. Methods

In order to assess future changes in wind energy, a multi-model ensemble (MME) of the GCMs that were found to best reproduce past-present data is constructed by means of the K—S, as explained in Section 2.2. The use of the MME has been proved to avoid individual uncertainties of the GMCs, therefore resulting in more reliable outcomes than single-model approaches (Räisänen and Palmer, 2001; Pierce et al., 2009). In this work, GCMs presenting over 60% of statistically similar points are merged into one MME following an unweighted approach (Carvalho et al., 2017; Tebaldi and Knutti, 1857). It is noteworthy that the selected models, i.e., NorESM2-MM, CESM2-waccm, EC-Earth3, GFDL-ESM4, GFDL-CM4, were found to best reproduce historical wind climate not only in North America (Table 2), but also in other regions, e.g., Europe (Martinez and Iglesias, 2021).

In order to fully understand the performance of the MME, the mean differences (bias) between the historical wind data of the MME and the ERA-5 database are assessed. Since this work considers a large range of latitudes, and the variability of the daily time series depends to a great extent on the latitude, the bias is normalised with the standard deviation of the sample (Brands et al., 2013) (Fig. 1). It is seen that the MME shows overall good agreement with the ERA-5 data on wind speed, especially in offshore locations and regions with few mountain ranges. However, large orographic features greatly influence the near-surface wind speed, as may be seen along the Pacific coast and the Rocky Mountains. Given the coarse resolution of the models involved in the study, none of them can simulate accurately terrain-induced modifications to the flow patters and thus large discrepancies are to be expected in mountain areas. (See Fig. 2.)

Wind power density (P) is computed as

$$P = \frac{1}{2}\rho U^3, \tag{1}$$

where U is the wind speed and ρ the air density (a value of 1.225 kg m^{-3} is assumed). By virtue of the cubic relationship between P and U, small changes in wind speed produce large changes in wind power density.

Two distinct time periods are considered to evaluate future changes in wind energy: mid-term future (2051-2060) and long-term future

Table 2
Number of grid points of the GCMs in the region studied statistically similar to their ERA-5 counterparts (percentage relative to the total number of grid points).

Model	Number of points statistically similar
NorESM2-MM	66%
CESM2-waccm	64%
EC-Earth3	64%
GFDL-ESM4	62%
GFDL-CM4	61%
ACCESS-CM2	59%
IPSL-CM6A-LR	57%
FGOALS-f3-L	56%
MPI-ESM1-2-HR	55%
AWI-CM-1-1-MR	55%
CanESM5	53%
BCC-CSM2-MR	51%
KACE-1-0-G	48%
MPI-ESM1-2-LR	47%
MRI-ESM2-0	47%
MIROC6	46%
INM-CM5-0	39%
INM-CM4-8	39%

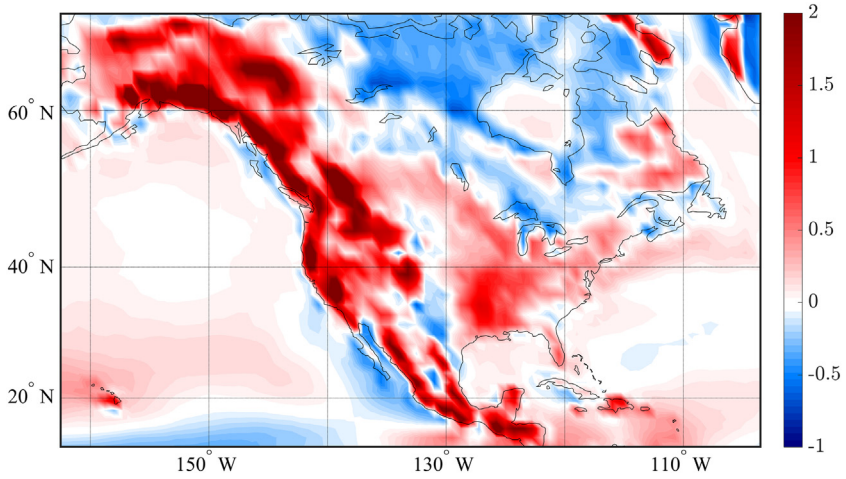

Fig. 1. Normalised bias of the multi-model ensemble historical data compared to the ERA-5.

(2091-2100). In the following, wind power density computed by the MME in the mid- and long-term future, in both climate change scenarios (SSP2-4.5 and SSP5-8.5) is compared with the values computed by the MME for the historical period (2005-2014) – hereinafter referred to as the baseline. The evolution of the wind energy resource is thus assessed as a percentage of change relative to the baseline values.

3. Results and discussion

3.1. Mean wind power density

Mean wind power density is computed for the mid- and long-term future in climate change scenarios SSP2-4.5 and SSP5-8.5 and compared with the baseline values. In the baseline, the large differences in the wind energy resource between onshore and offshore regions become apparent (Fig. 1). Due to the absence of land masses, the greater values of the mean wind power density (>200 Wm^{-2}) are located offshore in both the Atlantic and the Pacific Oceans. Especially prominent values of the mean wind power density (>400 Wm^{-2}) are found in latitudes over the 40th parallel, where the prevailing westerlies give rise to the most energetic winds and waves in the Northern Hemisphere (Zheng et al., 2018; Martinez and Iglesias, 2020). Onshore values of mean wind power density are below 200 Wm^{-2}.

Importantly, both climate change scenarios anticipate important changes in wind power density in the mid-term future (in the range of ±20%) and the long-term future (up to ±40%). The trends detected in the mid-term future in a particular area, whether positive or negative, are typically expanded in the long term.

The climate change scenario with intensive GHG emissions (SSP5-8.5) leads to the greatest changes in wind power density, in the range −40% to +30% in the long-term future. Climate projections in this scenario present a well-spread drop of ~15% in wind power density in the United States and Canada. Greater reductions in mean wind power density (~40%) are projected for Quebec and Nunavut, in Canada, and the US state of Alaska. Offshore locations, including the Hawaiian Islands, also present an overall decrease in this scenario, up to 15%.

Conversely, substantial increases in wind power density are predicted in the same climate change scenario (SSP5-8.5) for certain regions: the state of Texas and northeastern Mexico (>10%), Hudson Bay (~30%) and the regions of southern Mexico and Central America (up to 40%).

In climate change scenario SSP2-4.5 smaller changes relative to the baseline may be expected. In agreement with SSP5-5.8, this scenario

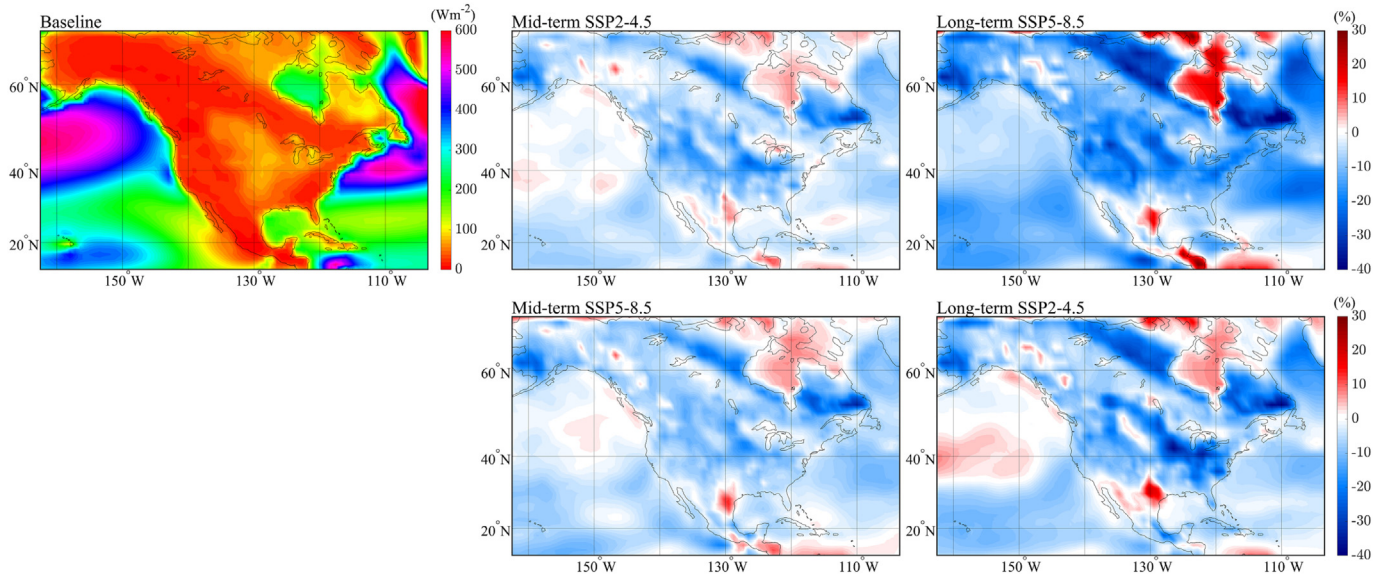

Fig. 2. Evolution of the mean wind power density in North America. Mean wind power density of the baseline (Wm^{-2}) and change (%) relative to the baseline in the mid- and long-term future for climate change scenarios SSP2-4.5 (upper panels) and SSP5-8.5 (lower panels).

projects a general decrease in wind power density in onshore territories, although of lesser magnitude. However, a more focused decrease in wind power density (up to 30%) is projected for the Eastern US and, especially, the midwestern states south of the Great Lakes, i.e., Wisconsin, Illinois, Michigan, Indiana and Ohio. Increases in wind power density are also predicted for certain areas, similar to those in climate change scenario SSP5-8.5, although less concentrated and of lesser magnitude.

Discrepancies between both climate change scenarios are found in Pacific offshore regions. Whereas SSP5-8.5 anticipates a substantial overall decrease, no general trend is discerned in SSP2-4.5. In the latter, slight increases and reductions in wind power density are found depending on the region considered.

Importantly, these results show changes of greater magnitude than previous works. In (Liu et al., 2014; Pryor and Barthelmie, 2011; Johnson and Erhardt, 2016), future changes in wind speed projected in the US in the late 21st century are of the order of 0.1-0.4 ms^{-1}. Little to no significant changes in wind speed were found in previous studies, based on the RCPs scenarios – the antecedents of the SSPs, which were used in the preceding phase of the Coupled Model Intercomparison Project Phase (CMIP5). In (Kulkarni and Huang, 2014), slight variations of ~5% in wind speed are estimated for the US territory, concluding that the current estimate of wind power will not shift significantly due to the action of GHG forcing. In (Costoya et al., 2020), a uniformly distributed decrease of 5% in wind speed is projected for the US east coast, and slight increases for the central regions of the US west coast.

The fact that with the SSPs scenarios of climate change greater changes are predicted than with the previous scenarios (RCPs) was also reported in other works. Results in (Martinez and Iglesias, 2021) demonstrate that the evolution of the European wind energy resource following the SSPs is more pronounced than considering the RCPs (Carvalho et al., 2017). It is clear that the more complex approach of the SSPs scenarios (Moss et al., 2010), integrating different socioeconomic factors which were previously disregarded, has led to greater changes in wind energy projections for a given GHG forcing.

3.2. Temporal variability of wind power density

The evolution of the temporal variability of the wind resource is studied by means of the coefficient of variation (COV), which is the ratio of the standard deviation (σ) to the mean value of a statistical sample (μ):

$$COV = \frac{\sigma}{\mu}. \quad (2)$$

Values of the COV are computed at each location in the mid- and long-term future projections and compared with the baseline (Fig. 3). In the baseline, the offshore wind resource is significantly more variable in latitudes over ~30° N in the Pacific Ocean and over ~25° N in the Atlantic. Onshore, the greatest variability is found along the East Coast of the United States and the northern and eastern Gulf Coast, which are affected by extratropical cyclones. Other foci of variability are located on the Pacific coasts of Canada and Central America.

Importantly for the energy sector, the temporal variability of the resource is predicted to increase generally in the long term in both climate change scenarios considered. In the mid-term projections, the coefficient of variation presents only small changes relative to the baseline, which can be either positive or negative depending on the region. However, the long-term projections anticipate widespread growth in the variability of the resource. Under climate change scenario SSP5-8.5, increases of up to 30% are predicted in the south of Ontario and Quebec. Offshore, a 20% increase in the COV is anticipated over the Pacific Ocean, including the Hawaiian Islands. Exceptionally, the variability is predicted to decrease in particular areas, including the Pacific coast of Mexico (up to 25%), Cuba (~10%) and the Caribbean Sea (~25%).

3.3. Intra-annual variability: seasonal mean wind power density

The evolution of the intra-annual variability of the wind energy resource is investigated by computing the seasonal mean wind power density values for the mid- and long-term projections and evaluating changes relative to the baseline values. In the study, four three-month seasons are considered: DJF (December – January – February), MMA (March – April – May), JJA (June –July – August) and SON (September – October – December).

In the baseline, significant seasonal variability of the resource is observed (Fig. 4). This is especially notable offshore in both the Atlantic and Pacific Oceans, with the highest values of wind power density (>900 Wm^{-2}) occurring in SON and, especially, DJF, matching the extratropical cyclone seasons of the Northern Hemisphere. By contrast, in JJA offshore values are below 350Wm^{-2}. This seasonality is also present onshore in the US and Canada, but to a far lesser extent.

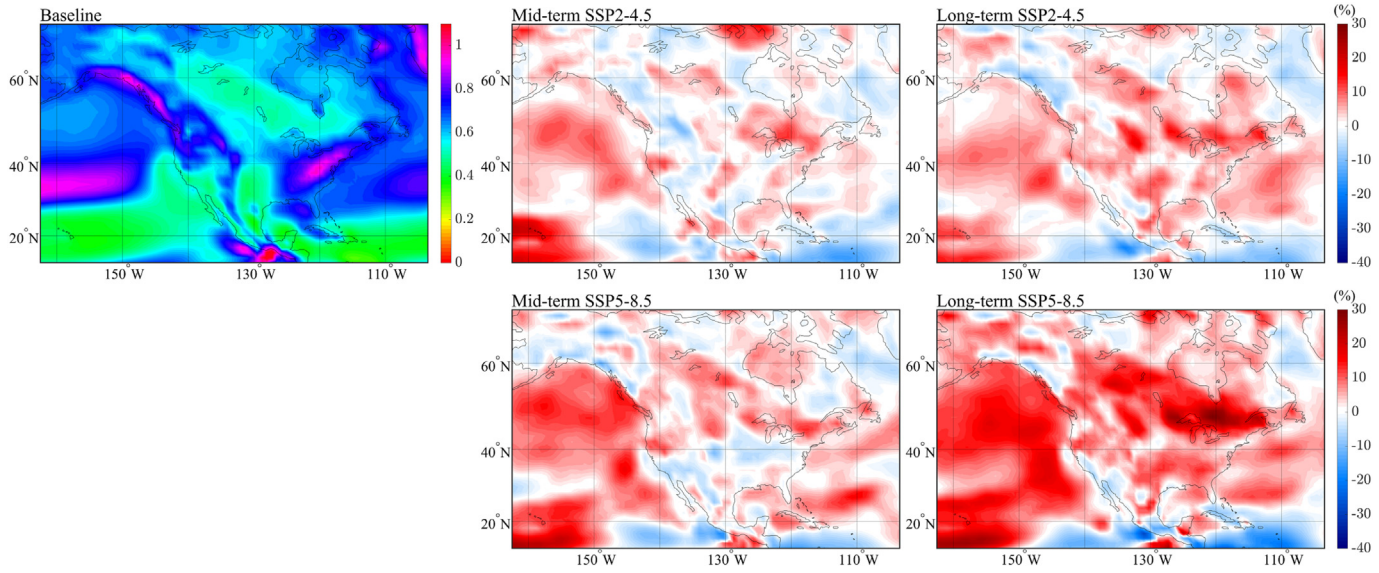

Fig. 3. Evolution of the temporal variability of wind power density in North America. Coefficient of variation (COV) of the baseline (upper-left panel) and change (%) relative to the baseline in the mid- and long-term future for climate change scenarios SSP2-4.5 (upper panels) and SSP5-8.5 (lower panels).

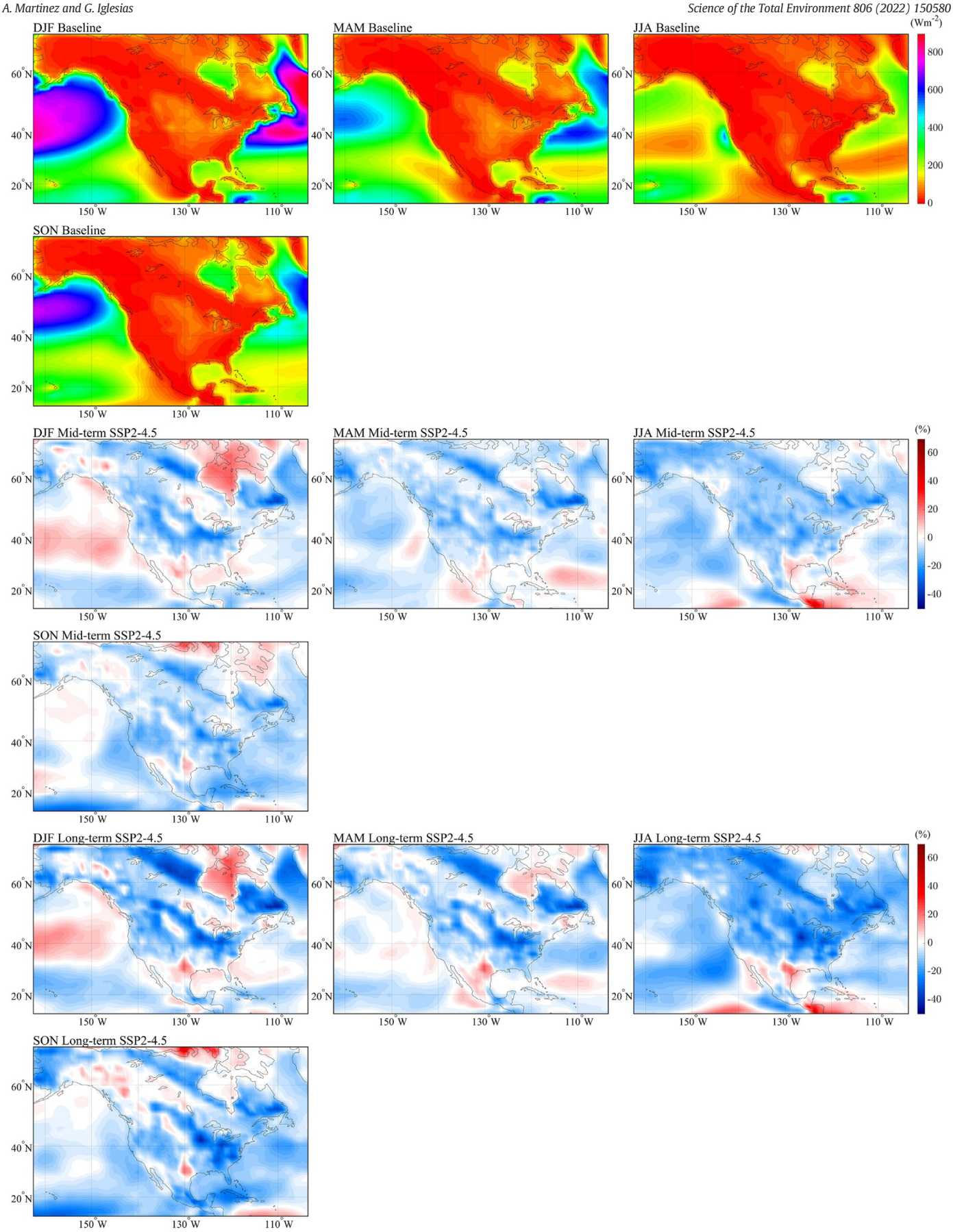

Fig. 4. Evolution of the seasonal mean wind power density in North America under climate change scenario SSP2-4.5. Historical (baseline) seasonal mean wind power density (Wm^{-2}, first and second rows of panels) and change (%) in the mid-term (third and fourth rows) and long-term (fifth and sixth rows) periods. DJF (December – January – February), MMA (March – April – May), JJA (June –July – August) and SON (September – October – December).

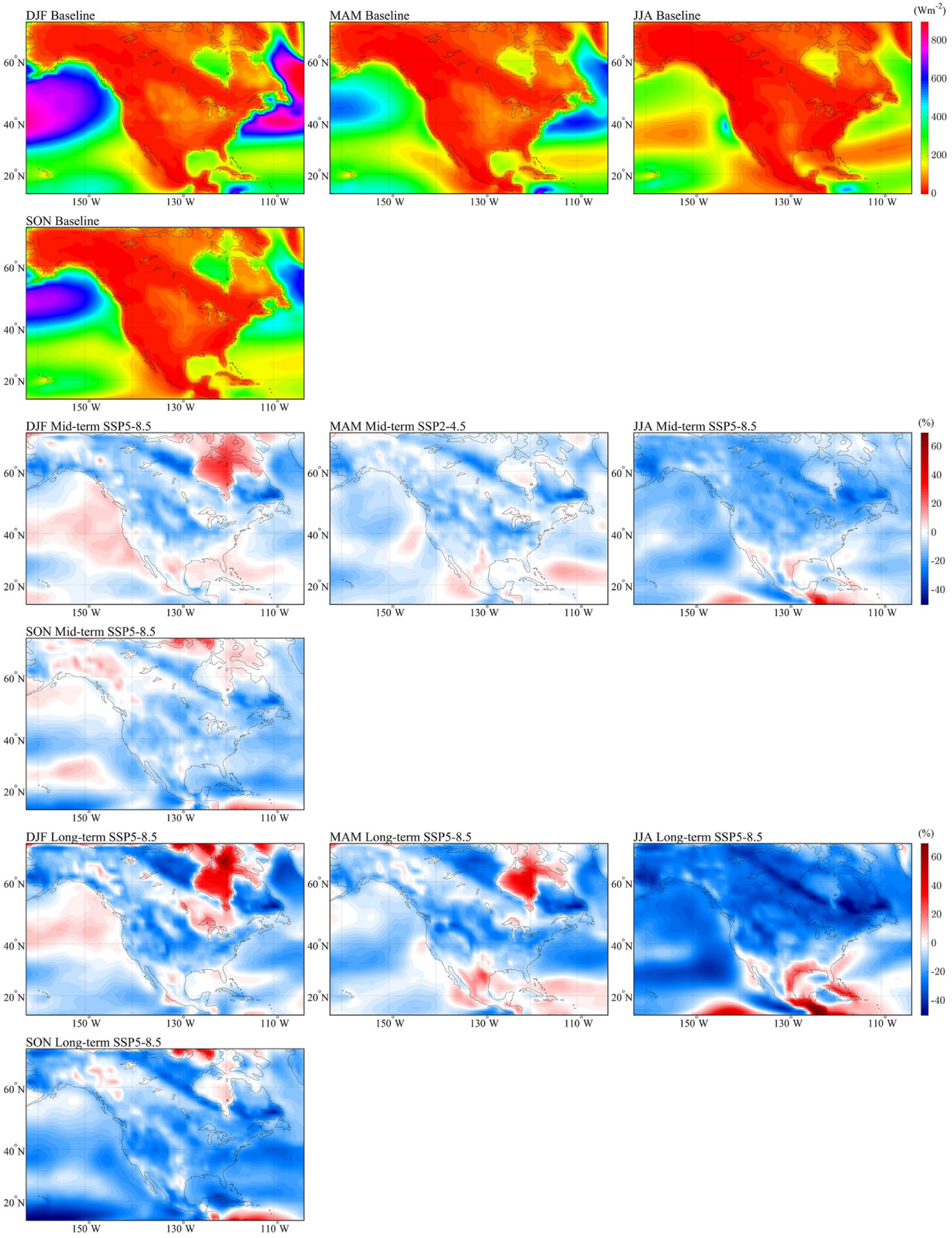
DJF Baseline
MAM Baseline
JJA Baseline
(Wm-2)
800
600
400
200
0
SON Baseline
DJF Mid-term SSP5-8.5
MAM Mid-term SSP2-4.5
JJA Mid-term SSP5-8.5
(%)
60
40
20
0
-20
-40
SON Mid-term SSP5-8.5
DJF Long-term SSP5-8.5
MAM Long-term SSP5-8.5
JJA Long-term SSP5-8.5
SON Long-term SSP5-8.5
60°N
40°N
20°N
150°W
130°W
110°W

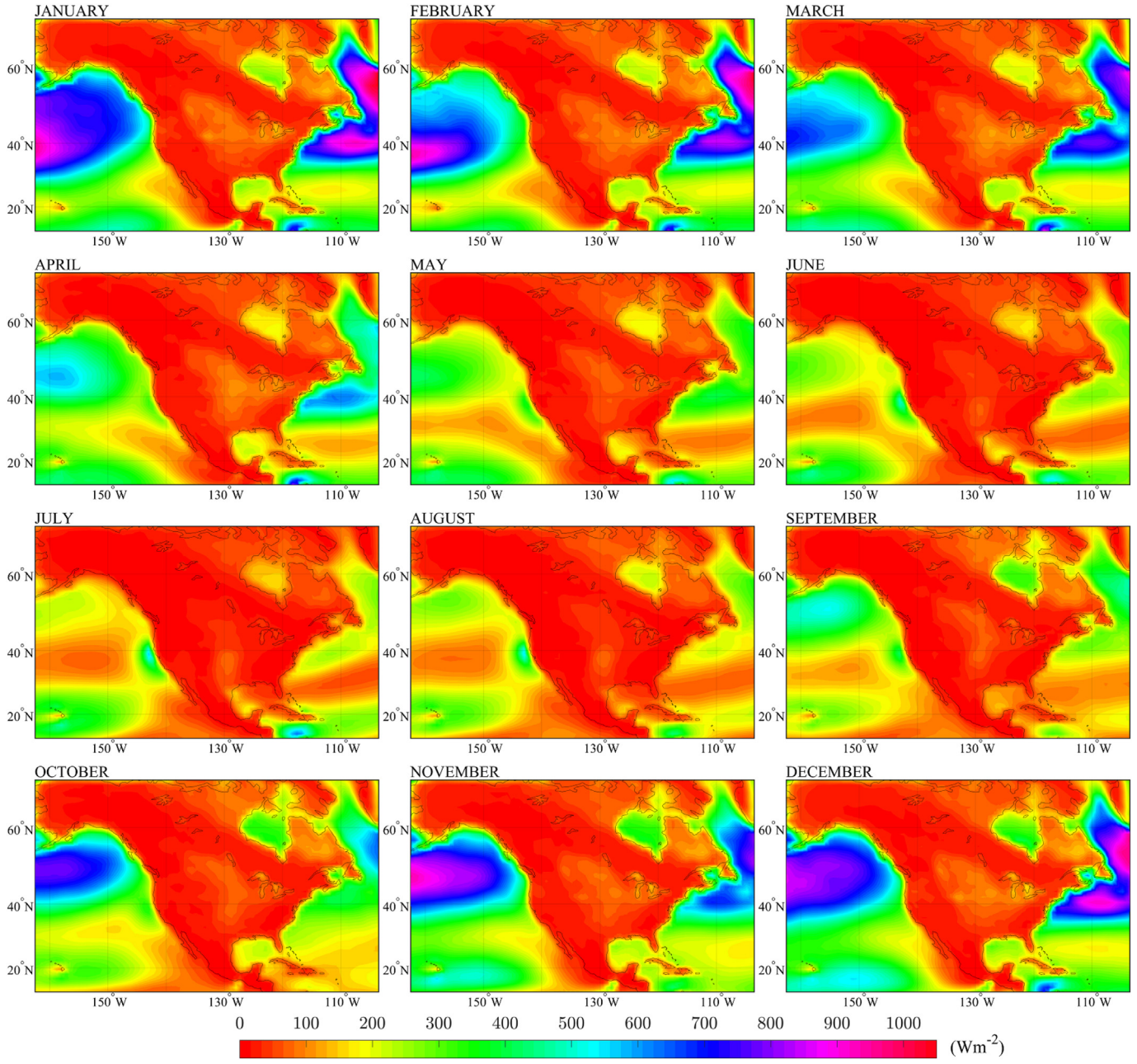

Fig. 6. Monthly mean wind power density, baseline (Wm^{-2}).

It is found that the evolution of the wind resource in both climate change scenarios SSP2-4.5 (Fig. 4) and SSP5-8.5 (Fig. 5) has itself a seasonal character, too. In SSP2-4.5, a strong rise in wind power density (up to 40%) is predicted in Hudson Bay in DJF and MAM, with no significant changes relative to the baseline in other seasons. In the Pacific Ocean, between parallels 30°N and 50°N, a general increase in wind power density (~10%) is projected exclusively in DJF. These increases in wind power density in DJF – a season that is already particularly energetic in the baseline – will exacerbate the intra-annual variability of the resource.

Certain changes observed in SSP2-4.5 are persistent throughout the year, e.g., the general decrease in wind power density in the US territory and the strong decrease (40%) in Quebec and Nunavut in Canada. Increases regardless of the season studied are anticipated in the US state of Texas and northern Mexico.

As regards SSP5-8.5, a much stronger seasonal evolution is apparent. A remarkable generalised drop in wind power density is predicted in JJA in latitudes greater than 35°N, especially in Nunavut and Quebec (up to 45%). However, in the same period strong increases (up to 80%) are predicted for the coastal regions of the Caribbean and, especially, southern Mexico and Central America. In DJF and MAM, a strong increase is located in Hudson Bay (of up to 45%).

In the offshore Pacific, strong drops in wind power density are predicted in JJA and SON (up to 45%), affecting the Hawaiian Islands to a

Fig. 5. Evolution of the seasonal mean wind power density in North America under climate change scenario SSP5-8.5. Historical (baseline) seasonal mean wind power density (Wm^{-2}, first and second rows of panels) and change (%) in the mid-term period (third and fourth rows) and long-term period (fifth and sixth rows). DJF (December – January – February), MMA (March – April – May), JJA (June –July – August) and SON (September – October – December).

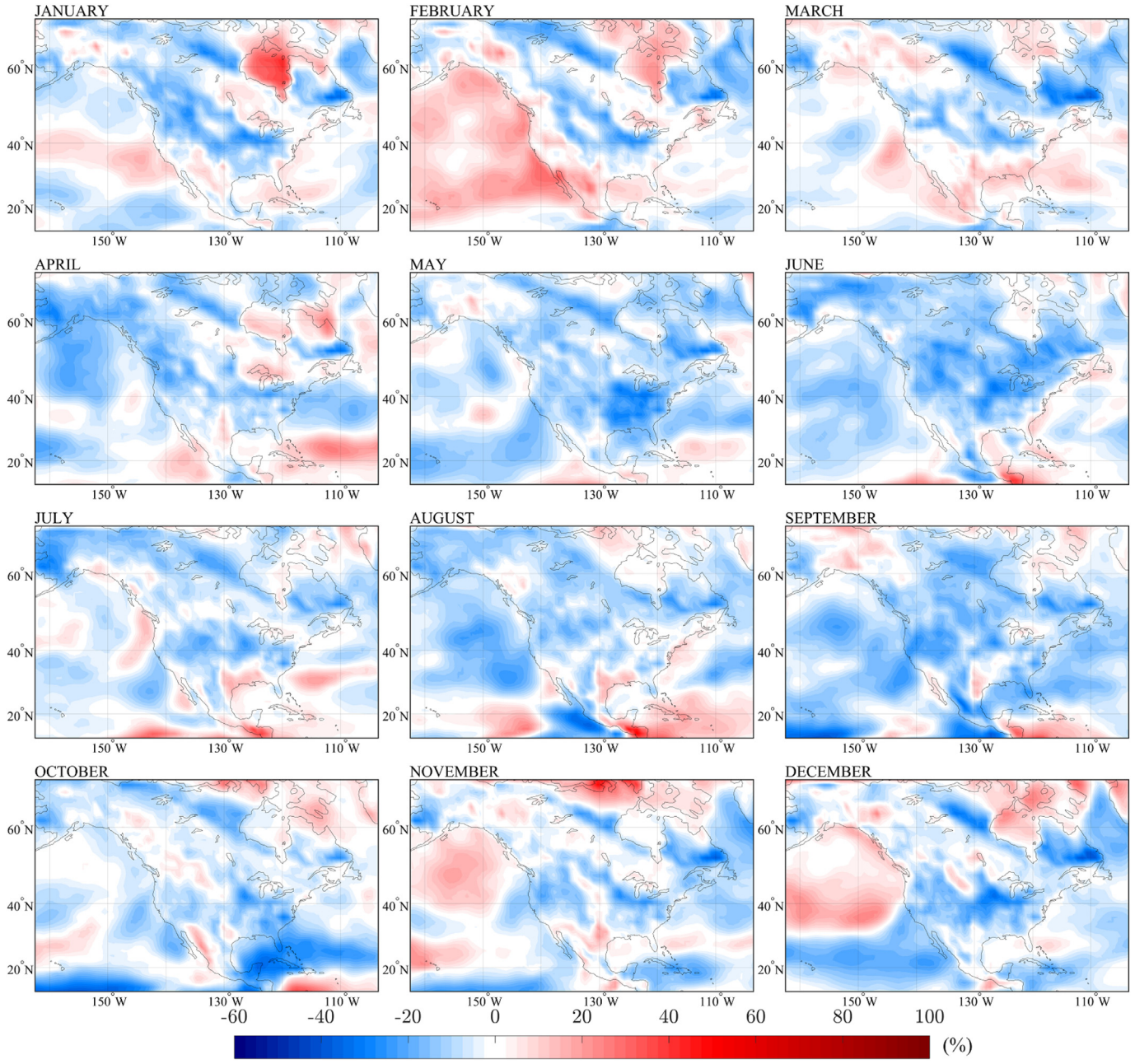

Fig. 7. Evolution (%) of the monthly mean wind power density in the mid-term future in climate change scenario SSP2-4.5 (relative to the baseline).

great extent. By contrast, no significant changes relative to the baseline are projected for DJF and MAJ.

The seasonal changes obtained in this work, based on CMIP6 data and SSP climate change scenarios, differ from previous studies based on CMIP5 data and RCP scenarios. In (Kulkarni and Huang, 2014), by considering different GCMs from the CMIP5, slight increases in wind power density were predicted in DJF in central regions of the US and small decreases in coastal regions in JJA for the RCP scenarios. It is apparent that the seasonal changes obtained in this work for the SSP scenarios are more pronounced.

3.4. Intra-annual variability: monthly mean wind power density

To study in depth the intra-annual variability in the evolution of the wind resource, in addition to the seasonal characterisation provided in the previous subsection, it is important to improve the temporal granularity by considering monthly mean values. The monthly mean wind power density in the mid- and long-term future is computed with the MME for both scenarios of climate change. The results are compared with the baseline values, and changes are represented as a percentage relative to the baseline.

In the baseline (Fig. 6), the most energetic winds (wind power density over 1100 Wm^{-2}) are found in offshore locations from October to March, matching the extratropical cyclone season. Onshore values are far smaller, below 200 Wm^{-2} throughout the year. The most energetic winds onshore occur in central parts of the continent, i.e., latitudes ranging from 40°N to 50°N and longitudes from 125°W to 135°W, particularly from November to April.

Climate change scenario SSP2-4.5 anticipates substantial changes in monthly mean wind power density in the mid-term (up to ±40%) (Fig. 7) and, especially, in the long-term (±50%) (Fig. 8). A remarkable increase in the intra-annual variability of wind power density is predicted in the Pacific coast of Mexico, with increases generally over 15% from February to August and, conversely, a strong decrease of up to

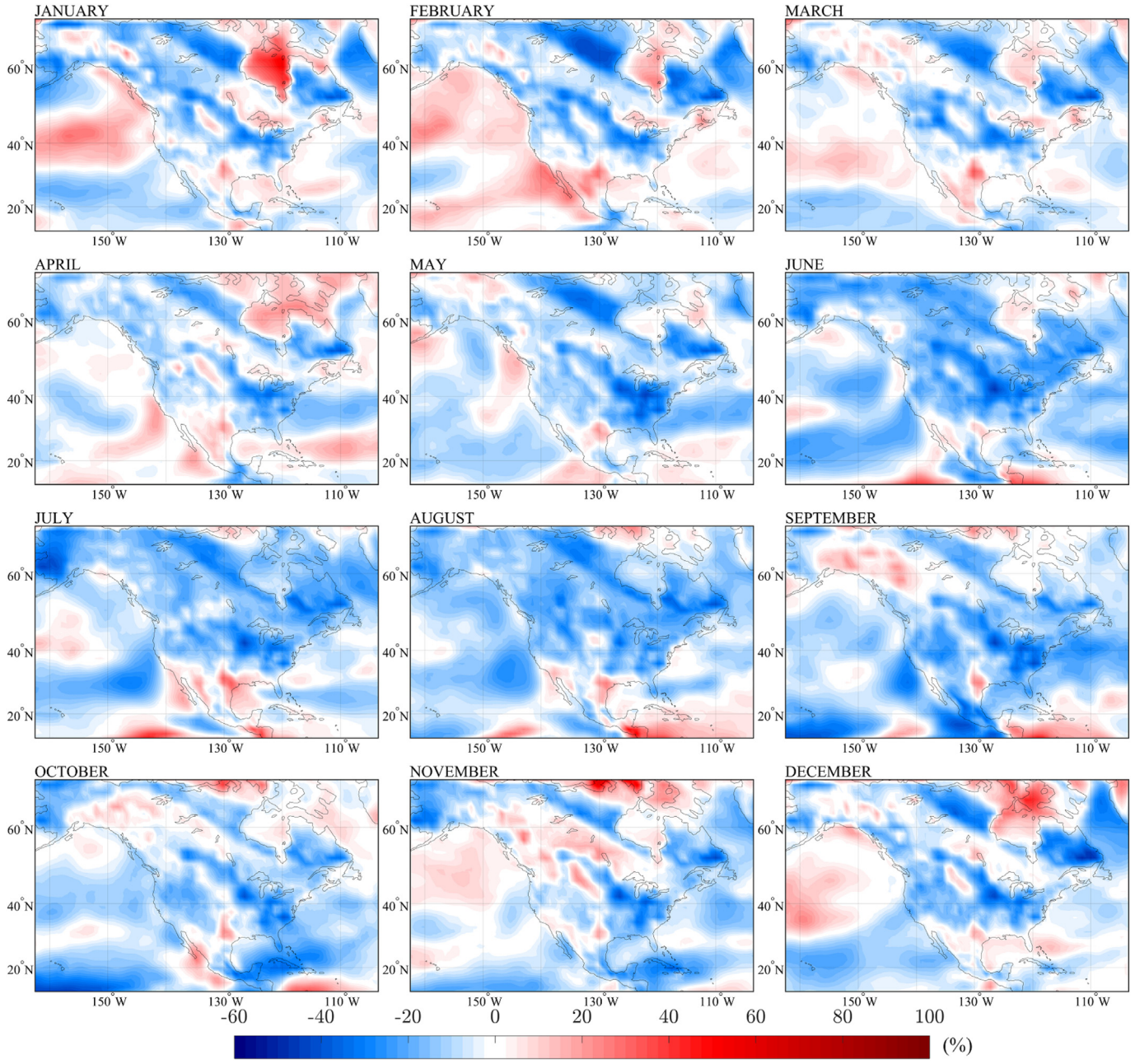

Fig. 8. Evolution (%) of the monthly mean wind power density in the long-term future in climate change scenario SSP2-4.5 (relative to the baseline).

40% in September. In offshore Pacific locations over the 35th parallel, a strong rise in wind power density is projected from November to March, surpassing 20% in December. Nonetheless, during the rest of the year, a small generalised drop is observed.

Importantly, climate change scenario SSP5-8.5 anticipates an even greater intra-annual variability than SSP2-4.5, as may be seen by comparing the colours between Figs. 9 and 7 (mid-term) and, especially, Figs. 10 and 8 (long-term) (note that the colour scale is the same in Figs. 7 to 10 to facilitate the comparison). Indeed, under SSP5-8.5, changes in monthly mean wind power density are substantial (-40% to 60%) in the mid-term (Fig. 9) and drastic (-60% to 120%) in the long-term future (Fig. 10). The greatest increases in wind power density (up to 120%) are predicted in southern Mexico and Central America from June to September, whereas the rest of the year little to no significant changes are observed. The same trend is observed in the Caribbean Sea, Cuba, the Gulf of Mexico, and the adjacent onshore territories (eastern Mexico and southeastern US), in which increases of up to 40% are predicted especially in August. In the case of Cuba, a strong decrease of 50% in wind power density is predicted solely in October. Substantial changes are also projected in Hudson Bay, with remarkable increases in the long-term future (of up to 80%) from January to April.

Finally, decreases in wind power density are predicted onshore, especially in latitudes greater than 35°N. According to the projections, these are more pronounced from May to September, with the reduction in wind power density reaching a hefty 60% in the aforementioned Quebec and Nunavut (Canada). In the offshore Pacific (including the Hawaiian Islands) a generalised drop of wind power density (up to 50%) is predicted from June to October.

4. Conclusions

The evolution of the wind resource in North America under the effects of climate change was investigated. Future projections of wind speed under the novel scenarios of climate change, the shared

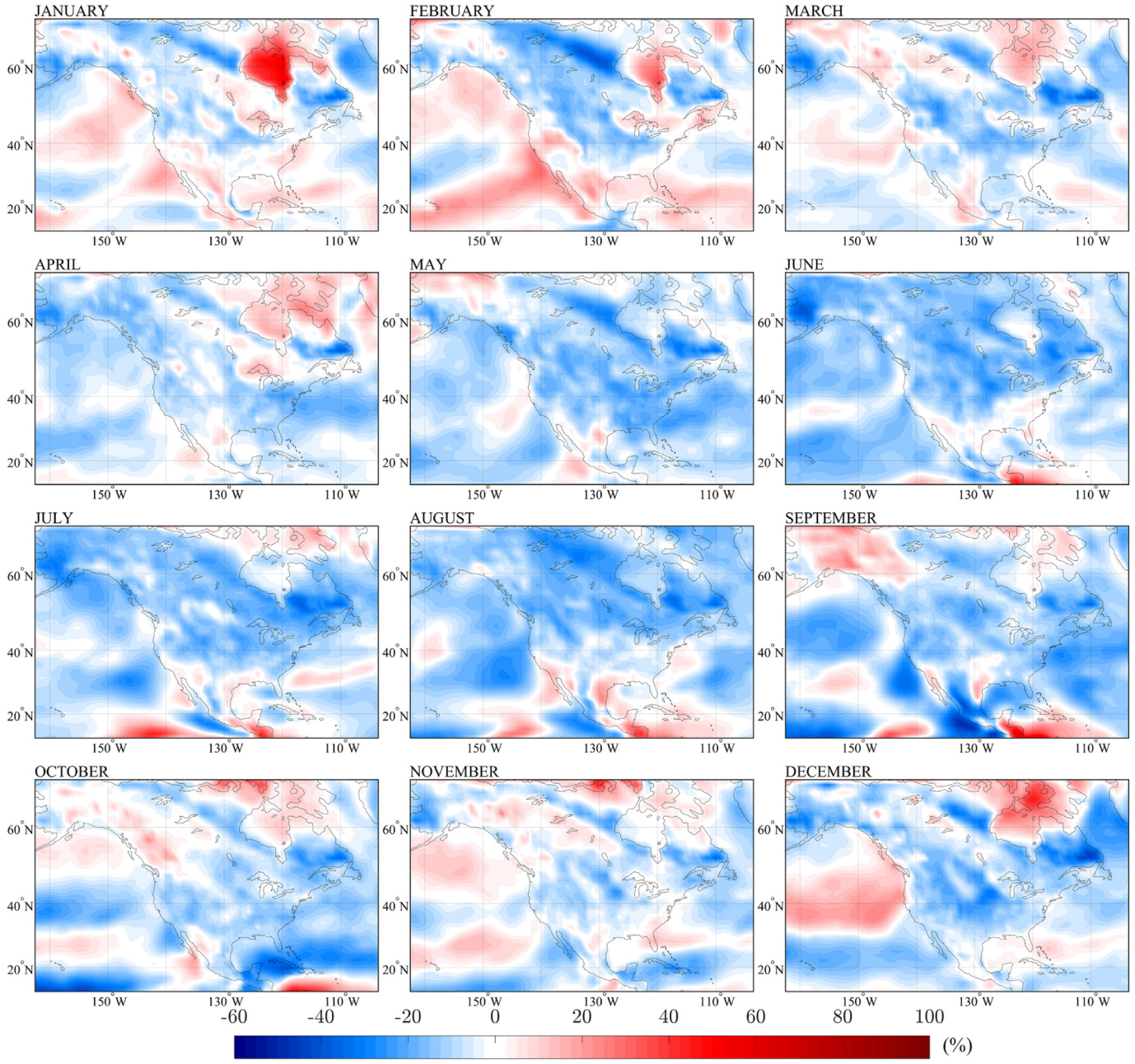

Fig. 9. Evolution (%) of the monthly mean wind power density in the mid-term future in climate change scenario SSP5-8.5 (relative to the baseline).

socioeconomic pathways (SSPs), were used for the analysis. 18 GCMs participating in the activities of the CMIP6 were considered, and the 5 GCMs that were found to best reproduce past-present wind conditions were chosen to construct a multi-model ensemble. In this manner, changes in wind power density relative to historical data (baseline) were assessed for the mid-term future (2051-2060) and long-term future (2091-2100) in two scenarios of climate change, SSP2-4.5 and SSP5-8.5.

Importantly, both climate change scenarios predict in the long-term future a well-spread drop in wind power density in the onshore territories of the US and Canada. In this period, the climate change scenario with intensive GHG emissions (SSP5-8.5) anticipates an overall decrease in mean wind power density of ~15% in these territories; if the rate of change were constant, this would imply a decadal decrease of ~2%. This reduction in mean wind power is most prominent in Quebec and Nunavut in Canada and in the US state of Alaska (up to 40%). Conversely, three foci of important increases in wind power density are anticipated in the long-term future in both climate change scenarios: the Hudson Bay (up to 25%), northern Mexico and the US state of Texas (up to 15%) and southern Mexico and Central America (up to 30%).

Discrepancies between the two climate change scenarios emerge in the Pacific Ocean, including the Hawaiian Islands. Whereas SSP5-8.5 anticipates an overall 15% decrease in mean wind power density, the evolution of the resource in SSP2-4.5 depends to a great extent on the region considered.

The strong seasonality detected in the evolution of the wind resource in climate change scenario SSP2-4.5 and, especially, SSP5-8.5 is most relevant to the intra-annual variability of the resource. In SSP5-8.5, substantial changes are predicted in average monthly wind power density in the long-term future, with increases surpassing 100% and decreases, 60%. These changes have a strong impact on

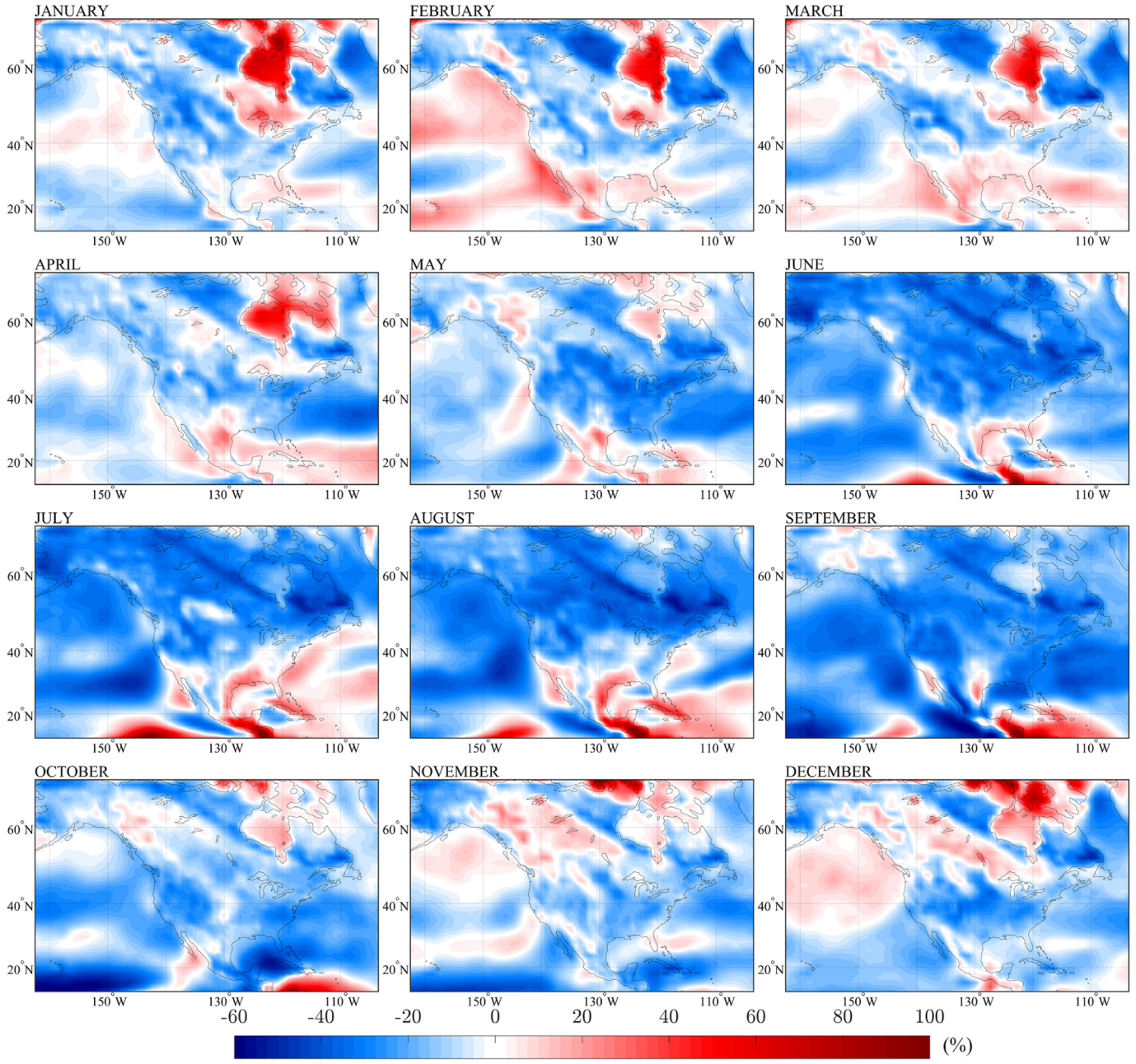

Fig. 10. Evolution (%) of the monthly mean wind power density in the long-term future in climate change scenario SSP5-8.5 (relative to the baseline).

the overall temporal variability of the resource, which are reflected on the coefficient of variability (COV). All in all, general increases in the COV of up to 15% and 30% are predicted in SSP2-4.5 and SSP5-8.5, respectively.

These results paint a picture of substantial changes in the wind resource that ought to be considered in the planning of the energy mix and future wind farm projects. For planning short to mid-term developments, e.g., new wind farms in the next 10-20 years, planners should consider primarily the mid-term results presented in this work. For making long-term estimates, for instance, about the evolution of the share of wind power within the energy mix, the long-term results are of greater significance. Although the multi-model ensemble approach eliminates individual biases and uncertainties to a great extent, some limitations of the GCMs are unavoidably inherited, such as the relatively coarse grid resolution or the inaccuracy in mountainous regions. Therefore, this large-scale evaluation should be complemented with regional-level studies for application at smaller (project) scale. Given that it is impossible to know at present which policies will be applied from now to 2100, and therefore which scenario corresponds better to the actual evolution that the wind resource will experience, the planning of wind power must consider the various possible courses of wind resource evolution under climate change.

CRediT authorship contribution statement

A. Martinez: Conceptualization, Methodology, Formal analysis, Investigation, Data curation, Writing – original draft. **G. Iglesias:** Conceptualization, Methodology, Writing – review & editing.

Declaration of competing interest

The authors declare that they have no known competing financial interests or personal relationships that could have appeared to influence the work reported in this paper.

Acknowledgements

The support of the Science Foundation Ireland (SFI) and the Marine Renewable Energy Centre Ireland (MaREI) is gratefully acknowledged (grant SFI MAREI2_12/RC/2302/P2 Platform RA). The authors are also grateful to: the World Climate Research Programme (WCRP), responsible for the CMIP6, and all the groups involved in its activities for producing and making available their works; the Earth System Grid Federation (ESGF), for making their data accessible; and the funding agencies supporting the WCRP and ESGF.

References

Astariz, S., Iglesias, G., 2016. Selecting optimum locations for co-located wave and wind energy farms. part II: a case study. Energy Convers. Manag. 122, 599–608.

Bentsen, M., Oliviè, D.J.L., Seland, Ø., Toniazzo, T., Gjermundsen, A., Graff, L.S., Debernard, J.B., Gupta, A.K., He, Y., Kirkevåg, A., Schwinger, J., Tjiputra, J., Aas, K.S., Bethke, I., Fan, Y., Griesfeller, J., Grini, A., Guo, C., Ilicak, M., Karset, I.H.H., Landgren, O.A., Liakka, J., Moseid, K.O., Nummelin, A., Spensberger, C., Tang, H., Zhang, Z., Heinze, C., Iversen, T., Schulz, M., 2019. NCC NorESM2-MM Model Output Prepared for CMIP6 CMIP. Earth System Grid Federation.

Bergillos, R.J., Rodriguez-Delgado, C., Allen, J., Iglesias, G., 2019. Wave energy converter geometry for coastal flooding mitigation. Sci. Total Environ. 668, 1232–1241.

Bloom, A., Kotroni, V., Lagouvardos, K., 2008. Climate change impact of wind energy availability in the eastern Mediterranean using the regional climate model PRECIS. Nat. Hazards Earth Syst. Sci. 8 (6).

Boucher, O., Denvil, S., Caubel, A., Foujols, M.A., 2019. IPSL IPSL-CM6A-LR Model Output Prepared for CMIP6 ScenarioMIP. Earth System Grid Federation.

Brands, S., Herrera, S., Fernández, J., Gutiérrez, J.M., 2013. How well do CMIP5 earth system models simulate present climate conditions in Europe and Africa? Clim. Dyn. 41 (3–4), 803–817.

Byun, Y.-H., Lim, Y.-J., Shim, S., Sung, H.M., Sun, M., Kim, J., Kim, B.-H., Lee, J.-H., Moon, H., 2019. NIMS-KMA KACE1.0-G Model Output Prepared for CMIP6 ScenarioMIP. Earth System Grid Federation.

CanWEA, 2021. Wind energy in Canada. https://canwea.ca/wind-energy/installed-capacity/.

Carvalho, D., Rocha, A., Gómez-Gesteira, M., Silva Santos, C., 2017. Potential impacts of climate change on european wind energy resource under the CMIP5 future climate projections. Renew. Energy 101, 29–40.

Castro-Santos, L., Filgueira-Vizoso, A., Carral-Couce, L., Formoso, J.Á.F., 2016. Economic feasibility of floating offshore wind farms. Energy 112, 868–882.

Château, P.-A., Chang, Y.-C., Chen, H., Ko, T.-T., 2012. Building a stakeholder's vision of an offshore wind-farm project: a group modeling approach. Sci. Total Environ. 420, 43–53.

Costoya, X., DeCastro, M., Carvalho, D., Gómez-Gesteira, M., 2020. On the suitability of offshore wind energy resource in the United States of America for the 21st century. Appl. Energy 262, 114537.

Danabasoglu, G., 2019. NCAR CESM2-WACCM Model Output Prepared for CMIP6 ScenarioMIP. Earth System Grid Federation.

Dix, M., Bi, D., Dobrohotoff, P., Fiedler, R., Harman, I., Law, R., Mackallah, C., Marsland, S., O'Farrell, S., Rashid, H., Srbinovsky, J., Sullivan, A., Trenham, C., Vohralik, P., Watterson, I., Williams, G., Woodhouse, M., Bodman, R., Dias, F.B., Domingues, C., Hannah, N., Heerdegen, A., Savita, A., Wales, S., Allen, C., Druken, K., Evans, B., Richards, C., Ridzwan, S.M., Roberts, D., Smillie, J., Snow, K., Ward, M., Yang, R., 2019. CSIRO-ARCCSS ACCESS-CM2 Model Output Prepared for CMIP6 ScenarioMIP. Earth System Grid Federation.

Dosio, A., Panitz, H.-J., Schubert-Frisius, M., Lüthi, D., 2015. Dynamical downscaling of CMIP5 global circulation models over CORDEX-Africa with COSMO-CLM: evaluation over the present climate and analysis of the added value. Clim. Dyn. 44 (9–10), 2637–2661.

EC-Earth Consortium, 2019. EC-Earth-Consortium EC-Earth3 Model Output Prepared for CMIP6 ScenarioMIP. Earth System Grid Federation.

Eyring, V., Bony, S., Meehl, G.A., Senior, C.A., Stevens, B., Stouffer, R.J., Taylor, K.E., 2016. Overview of the coupled model intercomparison project phase 6 (CMIP6) experimental design and organization. Geosci. Model Dev. 9 (5), 1937–1958.

Global Wind Energy Council, 2021. GWEC| Global Wind Report 2021.

Greaves, D., Iglesias, G., 2018. Wave and Tidal Energy. John Wiley & Sons.

Guo, H., John, J.G., Blanton, C., McHugh, C., Nikonov, S., Radhakrishnan, A., Zadeh, N.T., Balaji, V., Durachta, J., Dupuis, C., Menzel, R., Robinson, T., Underwood, S., Vahlenkamp, H., Dunne, K.A., Gauthier, P.P.G., Ginoux, P., Griffies, S.M., Hallberg, R., Harrison, M., Hurlin, W., Lin, P., Malyshev, S., Naik, V., Paulot, F., Paynter, D.J., Ploshay, J., Schwarzkopf, D.M., Seman, C.J., Shao, A., Silvers, L., Wyman, B., Yan, X., Zeng, Y., Adcroft, A., Dunne, J.P., Held, I.M., Krasting, J.P., Horowitz, L.W., Milly, C., Shevliakova, E., Winton, M., Zhao, M., Zhang, R., 2018. NOAA-GFDL GFDL-CM4 Model Output Prepared for CMIP6 ScenarioMIP. Earth System Grid Federation.

Gutowski, W.J., Giorgi, F., Timbal, B., Frigon, A., Jacob, D., Kang, H.-S., Raghavan, K., Lee, B., Lennard, C., Nikulin, G., 2016. WCRP Coordinated Regional Downscaling Experiment (CORDEX): A Diagnostic MIP for CMIP6.

Hernández-Escobedo, Q., Perea-Moreno, A.-J., Manzano-Agugliaro, F., 2018. Wind energy research in Mexico. Renew. Energy 123, 719–729.

Hersbach, H., Dee, D., 2016. ERA5 reanalysis is in production. ECMWF Newsl. 147 (7), 5–6.

IPCC, 2001. Climate Change 2001: The Scientific Basis. Cambridge University Press, Cambridge, UK, p. 881.

John, J.G., Blanton, C., McHugh, C., Radhakrishnan, A., Rand, K., Vahlenkamp, H., Wilson, C., Zadeh, N.T., Gauthier, P.P.G., Dunne, J.P., Dussin, R., Horowitz, L.W., Lin, P., Malyshev, S., Naik, V., Ploshay, J., Silvers, L., Stock, C., Winton, M., Zeng, Y., 2018. NOAA-GFDL GFDL-ESM4 Model Output Prepared for CMIP6 ScenarioMIP. Earth System Grid Federation.

Johnson, D.L., Erhardt, R.J., 2016. Projected impacts of climate change on wind energy density in the United States. Renew. Energy 85, 66–73.

Jones, P.W., 1999. First-and second-order conservative remapping schemes for grids in spherical coordinates. Mon. Weather Rev. 127 (9), 2204–2210.

Jonkman, J., Matha, D., 2010. Quantitative Comparison of the Responses of Three Floating Platforms. National Renewable Energy Lab.(NREL), Golden, CO (United States).

Kulkarni, S., Huang, H.-P., 2014. Changes in surface wind speed over North America from CMIP5 model projections and implications for wind energy. Adv. Meteorol. 2014, 292768.

Liu, B., Costa, K.B., Xie, L., Semazzi, F.H., 2014. Dynamical downscaling of climate change impacts on wind energy resources in the contiguous United States by using a limited-area model with scale-selective data assimilation. Adv. Meteorol. 2014.

López, M., Rodríguez, N., Iglesias, G., 2020. Combined floating offshore wind and solar PV. J. Mar. Sci. Eng. 8 (8), 576.

Martinez, A., Iglesias, G., 2020. Wave exploitability index and wave resource classification. Renew. Sust. Energ. Rev. 134, 110393.

Martinez, A., Iglesias, G., 2021. Wind resource evolution in Europe under different scenarios of climate change characterised by the novel shared socioeconomic pathways. Energy Convers. Manag. 234, 113961.

McInnes, K.L., Erwin, T.A., Bathols, J.M., 2011. Global climate model projected changes in 10 m wind speed and direction due to anthropogenic climate change. Atmos. Sci. Lett. 12 (4), 325–333.

Mordor Intelligence, 2021. North America wind power market - growth, trends, COVID-19 impact, and forecasts (2021 - 2026). https://www.mordorintelligence.com/industry-reports/north-america-wind-power-market#faqs.

Moss, R.H., Edmonds, J.A., Hibbard, K.A., Manning, M.R., Rose, S.K., Van Vuuren, D.P., Carter, T.R., Emori, S., Kainuma, M., Kram, T., 2010. The next generation of scenarios for climate change research and assessment. Nature 463 (7282), 747–756.

Negro, V., López-Gutiérrez, J.-S., Esteban, M.D., Alberdi, P., Imaz, M., Serraclara, J.-M., 2017. Monopiles in offshore wind: preliminary estimate of main dimensions. Ocean Eng. 133, 253–261.

O'Neill, B.C., Tebaldi, C., Vuuren, D.P.Van, Eyring, V., Friedlingstein, P., Hurtt, G., Knutti, R., Kriegler, E., Lamarque, J.-F., Lowe, J., 2016. The Scenario Model Intercomparison Project (ScenarioMIP) for CMIP6.

Perez-Collazo, C., Greaves, D., Iglesias, G., 2018. A novel hybrid wind-wave energy converter for jacket-frame substructures. Energies 11 (3), 637.

Perez-Collazo, C., Pemberton, R., Greaves, D., Iglesias, G., 2019. Monopile-mounted wave energy converter for a hybrid wind-wave system. Energy Convers. Manag. 199, 111971.

Pierce, D.W., Barnett, T.P., Santer, B.D., Gleckler, P.J., 2009. Selecting global climate models for regional climate change studies. Proc. Natl. Acad. Sci. 106 (21), 8441–8446.

Pınarbaşı, K., Galparsoro, I., Depellegrin, D., Bald, J., Pérez-Morán, G., Borja, Á., 2019. A modelling approach for offshore wind farm feasibility with respect to ecosystem-based marine spatial planning. Sci. Total Environ. 667, 306–317.

Pryor, S., Barthelmie, R., 2011. Assessing climate change impacts on the near-term stability of the wind energy resource over the United States. Proc. Natl. Acad. Sci. 108 (20), 8167–8171.

Qian, H., Zhang, R., 2021. Future changes in wind energy resource over the Northwest Passage based on the CMIP6 climate projections. Int. J. Energy Res. 45 (1), 920–937.

Räisänen, J., Palmer, T., 2001. A probability and decision-model analysis of a multimodel ensemble of climate change simulations. J. Clim. 14 (15), 3212–3226.

Räisänen, J., Hansson, U., Ullerstig, A., Döscher, R., Graham, L., Jones, C., Meier, H., Samuelsson, P., Willén, U., 2004. European climate in the late twenty-first century: regional simulations with two driving global models and two forcing scenarios. Clim. Dyn. 22 (1), 13–31.

Ramos, V., Carballo, R., Sanchez, M., Veigas, M., Iglesias, G., 2014. Tidal stream energy impacts on estuarine circulation. Energy Convers. Manag. 80, 137–149.

Rand, J., Hoen, B., 2017. Thirty years of north american wind energy acceptance research: what have we learned? Energy Res. Soc. Sci. 29, 135–148.

Riahi, K., Vuuren, D.P.Van, Kriegler, E., Edmonds, J., O'neill, B.C., Fujimori, S., Bauer, N., Calvin, K., Dellink, R., Fricko, O., 2017. The shared socioeconomic pathways and their energy, land use, and greenhouse gas emissions implications: an overview. Glob. Environ. Chang. 42, 153–168.

Rockel, B., Woth, K., 2007. Extremes of near-surface wind speed over Europe and their future changes as estimated from an ensemble of RCM simulations. Clim. Chang. 81 (1), 267–280.

Rodriguez-Delgado, C., Bergillos, R.J., Ortega-Sánchez, M., Iglesias, G., 2018. Wave farm effects on the coast: the alongshore position. Sci. Total Environ. 640, 1176–1186.

Schupfner, M., Wieners, K.-H., Wachsmann, F., Steger, C., Bittner, M., Jungclaus, J., Früh, B., Pankatz, K., Giorgetta, M., Reick, C., Legutke, S., Esch, M., Gayler, V., Haak, H., de Vrese, P., Raddatz, T., Mauritsen, T., von Storch, J.-S., Behrens, J., Brovkin, V., Claussen, M., Crueger, T., Fast, I., Fiedler, S., Hagemann, S., Hohenegger, C., Jahns, T., Kloster, S., Kinne, S., Lasslop, G., Kornblueh, L., Marotzke, J., Matei, D., Meraner, K., Mikolajewicz, U., Modali, K., Müller, W., Nabel, J., Notz, D., Peters, K., Pincus, R., Pohlmann, H., Pongratz, J., Rast, S., Schmidt, H., Schnur, R., Schulzweida, U., Six, K., Stevens, B., Voigt, A., Roeckner, E., 2019. DKRZ MPI-ESM1.2-HR Model Output Prepared for CMIP6 ScenarioMIP. Earth System Grid Federation.

Sclavounos, P., Lee, S., DiPietro, J., Potenza, G., Caramuscio, P., Michele, G.De, 2010. Floating offshore wind turbines: tension leg platform and taught leg buoy concepts supporting 3-5 MW wind turbines. European Wind Energy Conference EWEC.

Semmler, T., Danilov, S., Rackow, T., Sidorenko, D., Barbi, D., Hegewald, J., Pradhan, H.K., Sein, D., Wang, Q., Jung, T., 2019. AWI AWI-CM1.1MR Model Output Prepared for CMIP6 ScenarioMIP. Earth System Grid Federation.

Shiogama, H., Abe, M., Tatebe, H., 2019. MIROC MIROC6 Model Output Prepared for CMIP6 ScenarioMIP. Earth System Grid Federation.

Stelzenmüller, V., Gimpel, A., Haslob, H., Letschert, J., Berkenhagen, J., Brüning, S., 2021. Sustainable co-location solutions for offshore wind farms and fisheries need to account for socio-ecological trade-offs. Sci. Total Environ. 776, 145918.

Swart, N.C., Cole, J.N.S., Kharin, V.V., Lazare, M., Scinocca, J.F., Gillett, N.P., Anstey, J., Arora, V., Christian, J.R., Jiao, Y., Lee, W.G., Majaess, F., Saenko, O.A., Seiler, C., Seinen, C., Shao, A., Solheim, L., von Salzen, K., Yang, D., Winter, B., Sigmond, M., 2019. CCCma CanESM5 Model Output Prepared for CMIP6 ScenarioMIP. Earth System Grid Federation.

Tebaldi, C., Knutti, R., 1857. The use of the multi-model ensemble in probabilistic climate projections. Philos. Trans. R. Soc. A Math. Phys. Eng. Sci. 2007 (365), 2053–2075.

Tomasicchio, G.R., D'Alessandro, F., Avossa, A.M., Riefolo, L., Musci, E., Ricciardelli, F., Vicinanza, D., 2018. Experimental modelling of the dynamic behaviour of a spar buoy wind turbine. Renew. Energy 127, 412–432.

Ulazia, A., Sáenz, J., Ibarra-Berastegui, G., González-Rojí, S.J., Carreno-Madinabeitia, S., 2017. Using 3DVAR data assimilation to measure offshore wind energy potential at different turbine heights in the West Mediterranean. Appl. Energy 208, 1232–1245.

Veigas, M., Iglesias, G., 2015. A hybrid wave-wind offshore farm for an island. Int. J. Green Energy 12 (6), 570–576.

Veigas, M., Lopez, M., Romillo, P., Carballo, R., Castro, A., Iglesias, G., 2015. A proposed wave farm on the galician coast. Energy Convers. Manag. 99, 102–111.

Volodin, E., Mortikov, E., Gritsun, A., Lykossov, V., Galin, V., Diansky, N., Gusev, A., Kostrykin, S., Iakovlev, N., Shestakova, A., Emelina, S., 2019. INM INM-CM4-8 Model Output Prepared for CMIP6 ScenarioMIP ssp245. Earth System Grid Federation.

Volodin, E., Mortikov, E., Gritsun, A., Lykossov, V., Galin, V., Diansky, N., Gusev, A., Kostrykin, S., Iakovlev, N., Shestakova, A., Emelina, S., 2019. INM INM-CM4-8 Model Output Prepared for CMIP6 ScenarioMIP ssp585. Earth System Grid Federation.

Volodin, E., Mortikov, E., Gritsun, A., Lykossov, V., Galin, V., Diansky, N., Gusev, A., Kostrykin, S., Iakovlev, N., Shestakova, A., Emelina, S., 2019. INM INM-CM5-0 Model Output Prepared for CMIP6 ScenarioMIP ssp245. Earth System Grid Federation.

Volodin, E., Mortikov, E., Gritsun, A., Lykossov, V., Galin, V., Diansky, N., Gusev, A., Kostrykin, S., Iakovlev, N., Shestakova, A., Emelina, S., 2019. INM INM-CM5-0 Model Output Prepared for CMIP6 ScenarioMIP ssp585. Earth System Grid Federation.

Wieners, K.-H., Giorgetta, M., Jungclaus, J., Reick, C., Esch, M., Bittner, M., Gayler, V., Haak, H., de Vrese, P., Raddatz, T., Mauritsen, T., von Storch, J.-S., Behrens, J., Brovkin, V., Claussen, M., Crueger, T., Fast, I., Fiedler, S., Hagemann, S., Hohenegger, C., Jahns, T., Kloster, S., Kinne, S., Lasslop, G., Kornblueh, L., Marotzke, J., Matei, D., Meraner, K., Mikolajewicz, U., Modali, K., Müller, W., Nabel, J., Notz, D., Peters, K., Pincus, R., Pohlmann, H., Pongratz, J., Rast, S., Schmidt, H., Schnur, R., Schulzweida, U., Six, K., Stevens, B., Voigt, A., Roeckner, E., 2019. MPI-M MPI-ESM1.2-LR Model Output Prepared for CMIP6 ScenarioMIP ssp245. Earth System Grid Federation.

Wieners, K.-H., Giorgetta, M., Jungclaus, J., Reick, C., Esch, M., Bittner, M., Gayler, V., Haak, H., de Vrese, P., Raddatz, T., Mauritsen, T., von Storch, J.-S., Behrens, J., Brovkin, V., Claussen, M., Crueger, T., Fast, I., Fiedler, S., Hagemann, S., Hohenegger, C., Jahns, T., Kloster, S., Kinne, S., Lasslop, G., Kornblueh, L., Marotzke, J., Matei, D., Meraner, K., Mikolajewicz, U., Modali, K., Müller, W., Nabel, J., Notz, D., Peters, K., Pincus, R., Pohlmann, H., Pongratz, J., Rast, S., Schmidt, H., Schnur, R., Schulzweida, U., Six, K., Stevens, B., Voigt, A., Roeckner, E., 2019. MPI-M MPI-ESM1.2-LR Model Output Prepared for CMIP6 ScenarioMIP ssp585. Earth System Grid Federation.

Wilks, D.S., 2011. Statistical Methods in the Atmospheric Sciences. Vol. 100. Academic press.

Wu, J., Shi, Y., Xu, Y., 2020. Evaluation and projection of surface wind speed over China based on CMIP6 GCMs. J. Geophys. Res. Atmos. 125 (22) p. e2020JD033611.

Xin, X., Wu, T., Shi, X., Zhang, F., Li, J., Chu, M., Liu, Q., Yan, J., Ma, Q., Wei, M., 2019. BCC BCC-CSM2MR Model Output Prepared for CMIP6 ScenarioMIP. Earth System Grid Federation.

Yu, Y., 2019. CAS FGOALS-f3-L Model Output Prepared for CMIP6 ScenarioMIP. Earth System Grid Federation.

Yukimoto, S., Koshiro, T., Kawai, H., Oshima, N., Yoshida, K., Urakawa, S., Tsujino, H., Deushi, M., Tanaka, T., Hosaka, M., Yoshimura, H., Shindo, E., Mizuta, R., Ishii, M., Obata, A., Adachi, Y., 2019. MRI MRI-ESM2.0 Model Output Prepared for CMIP6 ScenarioMIP. Earth System Grid Federation.

Zhang, S., Li, X., 2021. Future projections of offshore wind energy resources in China using CMIP6 simulations and a deep learning-based downscaling method. Energy 217, 119321.

Zheng, C.-W., Xiao, Z.-N., Peng, Y.-H., Li, C.-Y., Du, Z.-B., 2018. Rezoning global offshore wind energy resources. Renew. Energy 129, 1–11.